Thermochimica Acta 491 (2009) 109–115

Contents lists available at ScienceDirect

Thermochimica Acta

journal homepage: www.elsevier.com/locate/tca

Observation of local heat release rate with changing combustor pressure in the CH_4/air flame (wrinkled laminar regime)☆

Jong-Ryul Kim[a], Fumiteru Akamatsu[b], Gyung-Min Choi[c,*], Duck-Jool Kim[c]

[a] Graduate School, Department of Mechanical Engineering, Pusan National University, 30 Jangjeon-dong, Gumjeong-ku, Busan 609-735, Republic of Korea
[b] Department of Mechanical Engineering, Osaka University, 1-1 Yamadaoka, Suita, Osaka 565-0871, Japan
[c] Pusan Clean Coal Center, Pusan National University, 30 Jangjeon-dong, Gumjeong-ku, Busan 609-735, Republic of Korea

ARTICLE INFO

Article history:
Received 30 July 2008
Received in revised form 20 March 2009
Accepted 24 March 2009
Available online 2 April 2009

Keywords:
Local heat release rate
Radical chemiluminescence intensity
Combustor pressure
Methane/air flame (wrinkled laminar regime)

ABSTRACT

The influence of combustor pressure on the local heat release rate of methane/air flames (wrinkled laminar regime) was investigated by measurements of local chemiluminescence intensity. Induced flow is often applied to the industrial boiler systems to improve heat transfer and prevent leakage of combustor. To investigate the combustion characteristics in the induced flow pattern, the pressure index (P^*) was controlled in the range of 0.7–1.3 for various equivalence ratio conditions for the present combustion system, where P^* is defined as the ratio of absolute pressure to atmospheric pressure. Relationships between local heat release rate and pressure index have been investigated by simultaneous measurements of C_2^*, CH^* and OH^* chemiluminescence intensities. Flame length became longer with decreasing P^*. The mean value of C_2^* and CH^*, which indicated the reaction intensity in the hydrocarbon flames, decreased with decreasing pressure index for $\Phi \leq 1$, but increased with decreasing pressure index for $\Phi > 1$. The C_2/CH value, which has a strong relationship with the local equivalence ratio, was almost the same for $\Phi \leq 1$, regardless of the change of the pressure index, but showed a large level for lower pressure index and $\Phi > 1$ conditions. For rich combustion conditions, a combustor pressure lower than the atmospheric pressure enhanced the combustion reaction by increasing the diffusion velocity of unburned fuel.

1. Introduction

Induced flow is often applied to the industrial boiler systems to improve heat transfer and prevent leakage. In the case of boiler using induced flow, there is pressure drop by several tens of Torr. The changing combustor pressure has a significant effect on the flame structure and emission characteristics even for a pressure change of only several tens of Torr. Generally, combustor pressure influences in the flame temperature and flame burning velocity.

The influence of the combustor pressure on the flame characteristics in an industrial boiler system has been investigated extensively. Liakos et al. [1] analyzed the mechanisms that control the premixed combustion phenomenon at different pressures (atmospheric and higher pressures) and investigated the effects of elevated pressure on the turbulence characteristic. It has been predicted that the size of the combustion zone is reduced with increased reactant pressure. Laminar burning velocity was measured by changing the equivalence ratio under a high-temperature and high-pressure condition. The laminar burning velocity decreased with increasing initial pressure at constant unburned gas temperature and increased at constant initial pressure with increasing unburned gas temperature [2]. A premixed flame code was used to investigate the NO formation in a series of lean-premixed $CH_4/O_2/N_2$ laminar flames at pressure of 1–14.6 atm [3]. In the high-pressure turbulent premixed flames, pressure increase caused a finer and more convoluted structure of the flame and the pressure had an extensive effect on the turbulent burning velocity [4]. However, most previous researches have been conducted for high-pressure conditions rather than atmospheric conditions. Therefore, in order to understand the details of the flame structure and establish a robust combustion control scheme for an induced flow pattern, it is necessary to investigate the combustion characteristics at low-pressure than at atmospheric pressure.

In general, an intrusive measurement method is desired for hot, erosive environment due to experimental limitations. The C_2^*, CH^* and OH^* chemiluminescence intensity can be used to observe the location of the primary combustion region in hydrocarbon flames. Particularly, the profile OH^* spectra has a strong relationship with the flame temperature, the heat release rate, and the thermal NO mechanism in hydrocarbon flames. The excited C_2^* free radical species is short-lived, and is also a good indicator of the reaction

☆ This paper was presented at 8th Symposium of the Korean Society of Thermophysical Properties held at POSTECH, Korea from April 24–25, 2008.

* Corresponding author. Tel.: +82 51 510 2476; fax: +82 51 516 5236.
E-mail address: choigm@pusan.ac.kr (G.-M. Choi).

0040-6031/$ – see front matter © 2009 Elsevier B.V. All rights reserved.
doi:10.1016/j.tca.2009.03.012

zone in rich flames. CH^* is considered a better tracer for observing the reaction zone and heat release of hydrocarbon flames [5–8].

Higgins et al. [9,10] found the linear relation of OH^* and CH^* chemiluminescence to equivalence ratio at $\Phi = 0.66–0.86$ and $P = 0.5–2.5$ MPa using line of sight measurements. CH chemiluminescence at high-pressure was found to have power law dependence with the equivalence ratio and pressure and be proportional to the mass flow rate. Ikeda et al. [11,12] investigated the spatially and spectrally resolved chemiluminescence spectra for high-pressure premixed methane air flames. They concluded that the background CO_2^* spectra, which are characterized by a broadband emission spectrum extending from 300 to 600 nm, became significant with increasing pressure. Doquire et al. [13] compared the characteristics of the local and the global intensity of excited OH^*, CH^* and C_2^* radicals in terms of the equivalence ratio (0.6–1.1) and pressure (1–10 bar) by experiments and computations methods. Experimental results showed that chemiluminescence was a good indicator for direct monitoring of the equivalence ratio, although this signal is strongly corrected with pressure. Chou and Patterson [14] used the optical fiber system to measure simultaneously C_2^* and CH^* signal positions of cylinder and also showed a relationship between the local A/F and the C_2^*/CH^* ratio. Ikeda et al. [15,16] found the ratio of the C_2^*/CH^* and the OH^*/CH^* versus local equivalence ratio for the local flame front of a laminar premixed flame was investigated and found a strong correlation. Recently, the relationships between the local heat release rate and CH concentration have investigated by numerical simulations of methane–air premixed flames, and simultaneous CH and OH PLIF (Planar laser-induced fluorescence) measurements have been also conducted for the laminar flame [17]. Choi et al. found that CH concentration is a good enough indicator of the local heat release rate in a turbulent premixed flame. Although PLIF is an available quantitative measure, radical chemiluminescence measurement provides more meaningful information in the understanding of the reaction characteristics of unsteady reacting flow.

The objectives of the present study are to investigate the flame structure and reaction characteristics at low combustor pressure rather than at atmospheric pressure. In this study, the flame structure and combustion characteristics with variation of combustor pressure from −30 kPa to 30 kPa (gage pressure) were investigated by visualization, mean temperature and NO_x emission measurements. The reaction characteristics were analyzed by measurements of CH^*, C_2^* and OH^* chemiluminescence intensities. The relationship between the local heat release rate and combustor pressure was discussed.

2. Experimental condition and method

Fig. 1(A) shows the schematic diagram of the combustion system with combustor pressure control. The combustor pressure was controlled by the flow rate balance between high-pressure blower at the upstream and vacuum pump at the downstream. For the measurement of the combustor pressure in the combustion chamber, a pressure transducer was installed 100 mm downstream from the main burner. The combustor pressure was normalized as a pressure index ($P^* = P_{abs}/P_{atm}$), where P_{abs} and P_{atm} indicate the absolute pressure and atmosphere pressure, respectively. Pressure index was controlled in the range of 0.7–1.3 for each equivalence ratio conditions.

Fig. 1(B) shows the schematics of the combustor and the detail of the nozzle. The inner cross-section of the combustion chamber was 55 mm × 55 mm and its length was 550 mm. On each side of the combustion chamber, silica glass plate of 300 mm × 55 mm and 5 mm thickness ($\lambda = 200–2000$ nm) was installed to allow optical access. A flame holder installed with a diffuser and pilot-flame

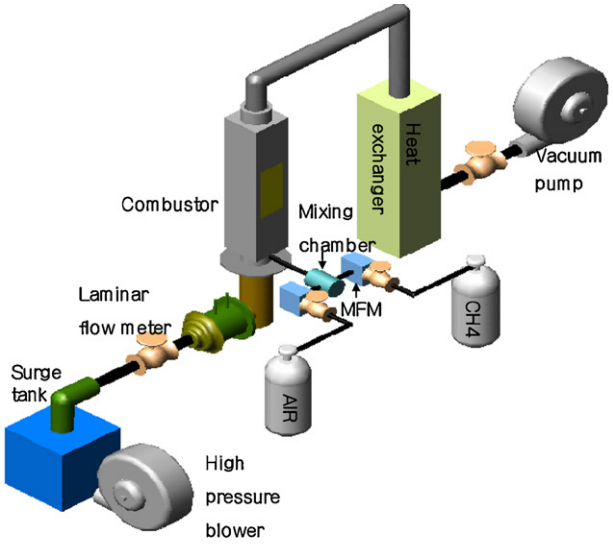

(A) Schematic of combustion system including pressure control system

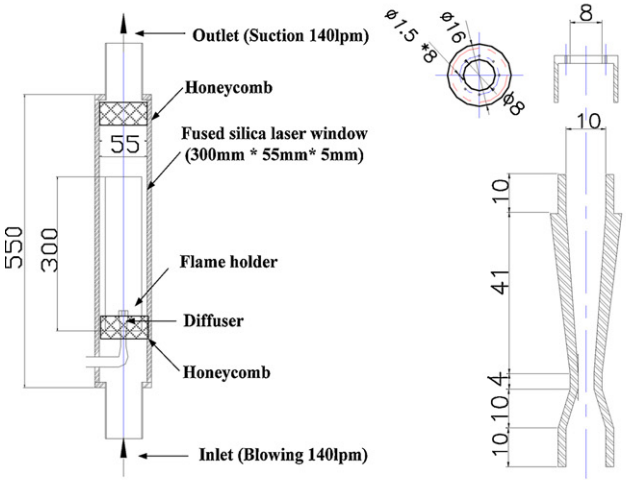

(B) Detail diagram of combustor and mixture nozzle

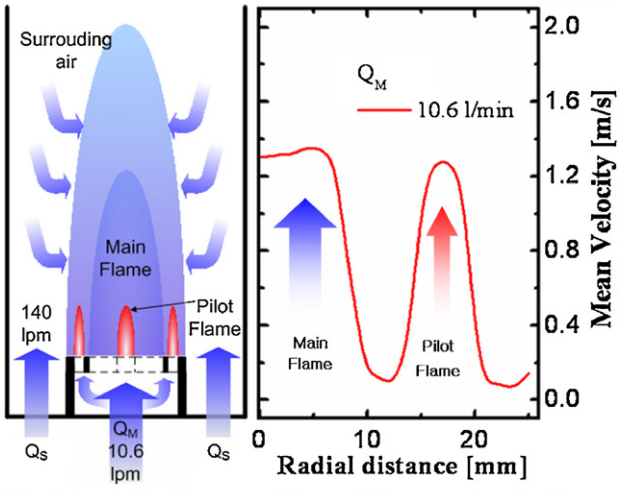

(C) Schematic diagram of formed flame and velocity profiles of main and pilot flame nozzles.

Fig. 1. Experimental setup in methane/air flame.

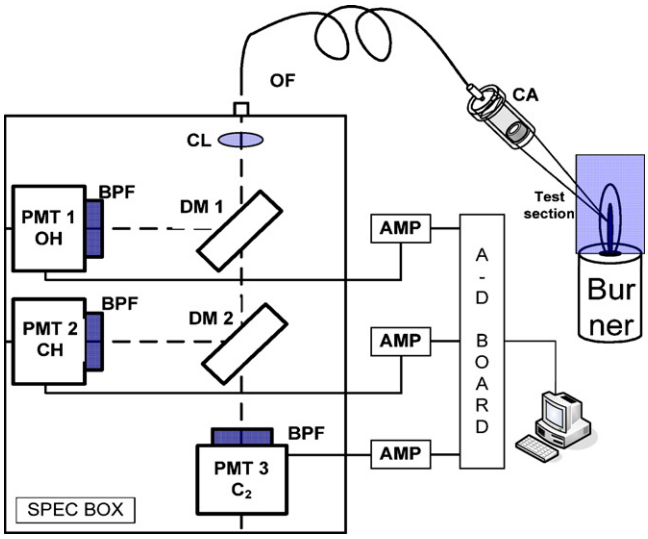

Fig. 2. Experimental setup for chemiluminescence spectra measurement in the methane/air flame.

injector was mounted to stabilize the flames against various changes of the combustor pressure. The flame holder had a main hole of 8 mm inner diameter, and a pilot flame hole was installed around the main hole, and its exit had 8 injection holes (ID = 1.5 mm). Steel balls and honeycomb were installed in the mixing chamber to rectify the flow of the mixture and to prevent flashback. The air and fuel were supplied to the mixing chamber through the mass flow controller (KOFLOC-3660). Equivalence ratios were controlled in the range of 0.9–1.2 by the air flow rate and the CH_4 flow rate. The mixture flow rates of the main hole and the pilot flame injector were 8.2 and 0.8 L/min, respectively. The mean velocity of the main mixture and its Reynolds number were 1.3 m/s and 696.2. And, the surrounding air was supplied at the same velocity as that of the main mixture (140 L/min). Fig. 1(C) shows the schematics diagram of the formed flame and the velocity profiles of the main and pilot nozzles.

The concentration of the nitric oxides was measured by a chemiluminescence gas analyzer (SHIMADZU, NOA-7000). Exhaust gases were sampled by a water-cooled gas sampling probe with a 1 mm sampling hole. Burned gas was sampled by a collection at 5 mm intervals on the central axis. Silica gel and gauze were used to trap soot and moisture. Measured values were expressed as $EINO_x$ [18,19]. Since the pressure index and the mixing of the main flame and surrounding air near the burner nozzle influenced the flame shape, $EINO_x$ was expressed as an averaged value of all measurement points along the central axis. Mean flame temperature was measured at a half length cross-section of flame length using a type-R (Pt/13%Rh) thermocouple of 0.1 mm wire diameter. Thirty holes (d = 5 mm) were installed at 10 mm intervals on the sidewall of the combustor for temperature measurements.

Fig. 2 shows the schematic diagram of the experimental setup for optical diagnostics. In the present study, the Cassegrain mirror

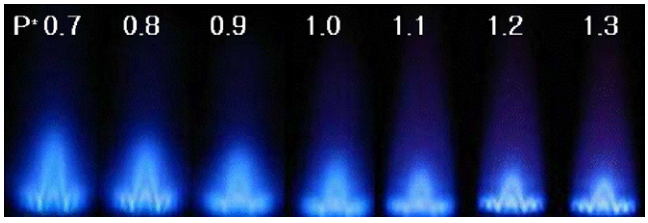

Fig. 3. Direct photographs of flame with changing combustor pressure (Φ = 1.0).

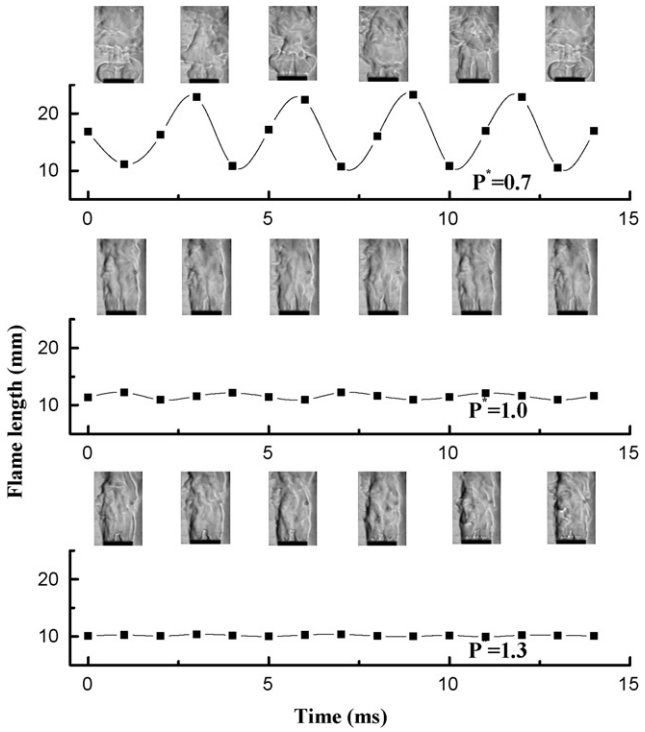

Fig. 4. Time-series flame length and schlieren photographs.

system was used for collecting flame emissions. Cassegrain optics achieves a very high spatial resolution by minimizing the spherical aberration between the pair of mirrors, and eliminating chromatic aberration [20]. The collected flame emissions were sent to the photomultiplier spectroscopic unit, which consists of optical band-pass filters and a photomultiplier (Hamamatsu, R106UH) for detecting the OH^*, CH^* and $C_2{}^*$ emission intensities. The specifications (center wavelength/FWHM/transmitting efficiency) of each optical filter are as follows: OH^*, 306 nm/14 nm/35%, CH^*, 431.4 nm/1.5 nm/49.2%, and $C_2{}^*$, 516.5 nm/2 nm/65%. The amplifier and photomultiplier gain were kept constant for all measurements [20,21].

The analog output signals from the photomultipliers were simultaneously amplified, filtered (LPF 1 kHz), and digitized by an A/D converter (NI-DAQ) at a sampling rate of 5 kHz.

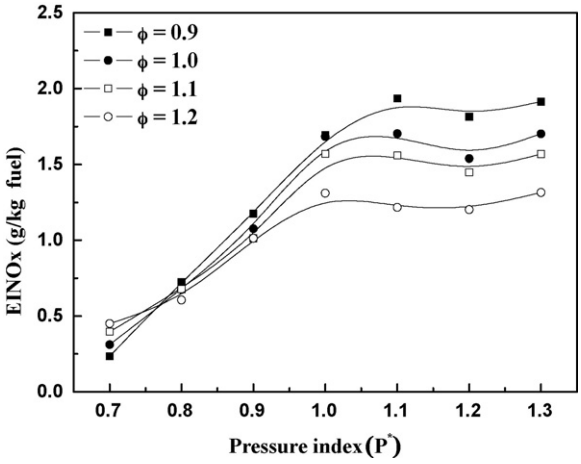

Fig. 5. Averaged nitric oxide emission as functions of pressure index and equivalence ratio.

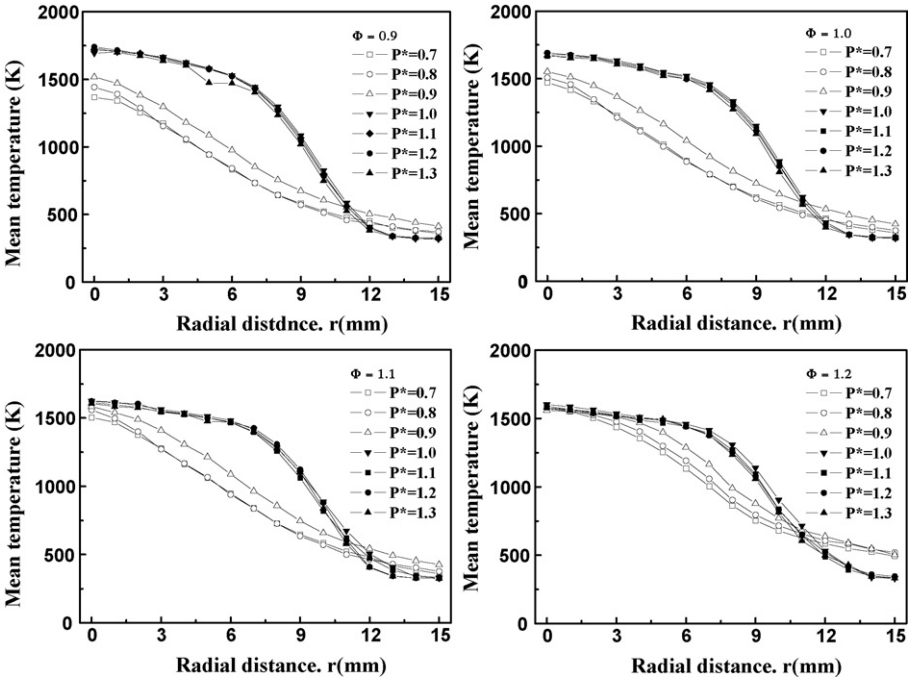

Fig. 6. Mean temperature distribution as functions of pressure index and equivalence ratio.

3. Results and discussion

3.1. Flame structure and emission index

Fig. 3 shows direct photographs of flames with the variation of the pressure index at $\Phi = 1.0$. In this combustion system, flames were stabilized until $P^* = 0.7$, regardless of the equivalence ratio. The flames have a double flame structure; the inner flame region was cone shaped and its color was bright blue. The outer flame region showed weak brightness of blue. The mixture injected from the flame holder initiated the primary combustion reaction in the inner flame region, and some unburned compositions started the secondary combustion reaction in the outer flame region. The inner flame length was increased, and the cone angle at the flame tip became smaller with decreasing pressure index. This phenomenon resulted from the decreased burning velocity and thermal diffusiv-

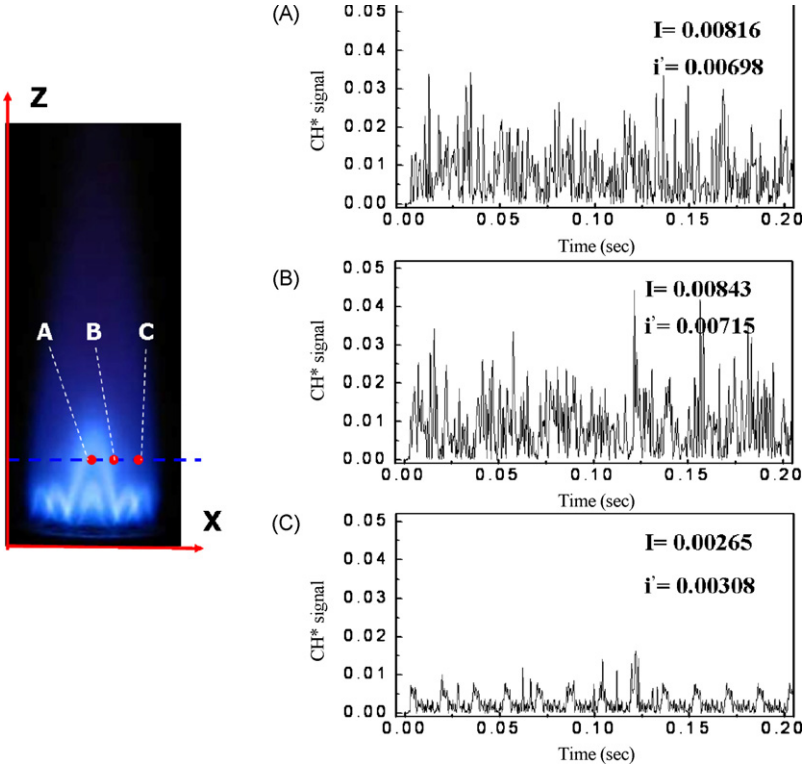

Fig. 7. Representative time-series signal of CH^* at the reaction zone.

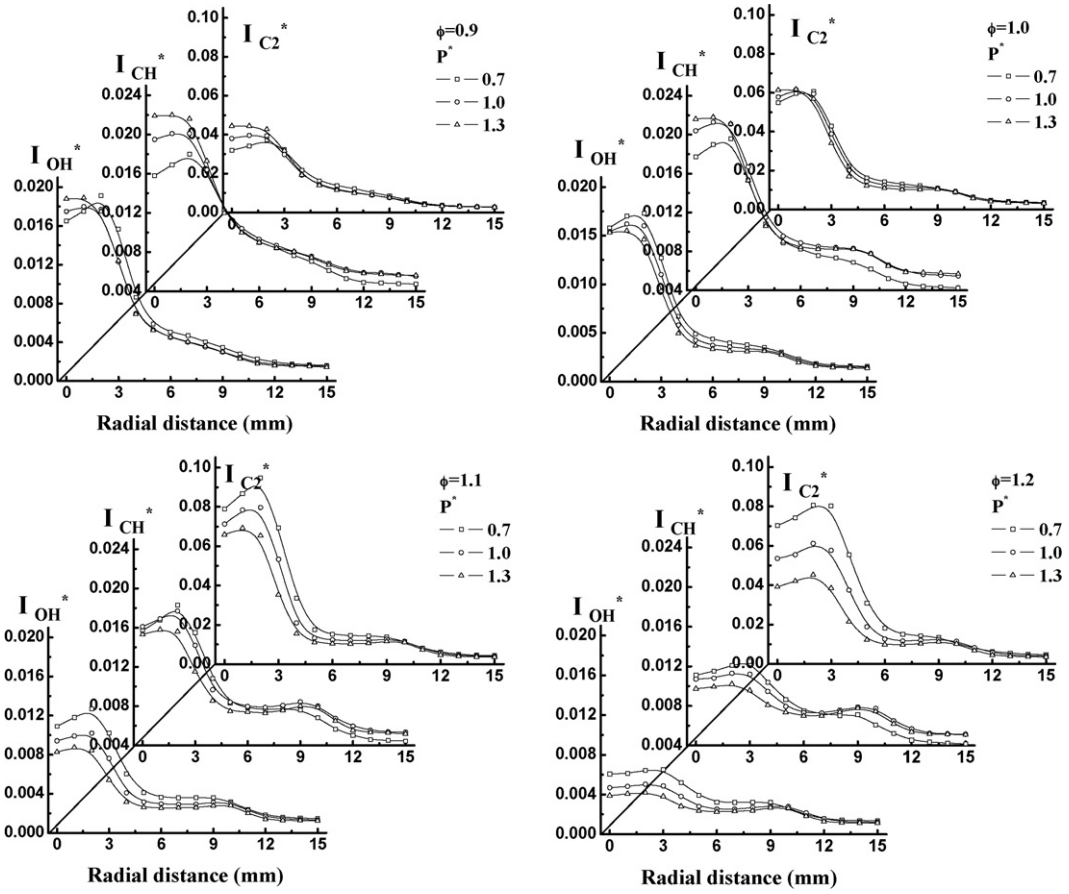

Fig. 8. Distributions of chemiluminescence intensities of OH^*, CH^* and $C_2{}^*$ as functions of pressure index and equivalence ratio.

ity with decreasing pressure index, and this tendency was similar to the results from Ref. [4,24].

Fig. 4 shows representative time-series schlieren photograph and fluctuations of inner flame length with the pressure index. It could be observed that pilot flame and the surrounding air moving into the inner flame in the $P^* \geq 1$ conditions and that surrounding air and flow pattern was widely dispersed in the $P^* < 1$ conditions. While the flame shape does not change significantly under the condition of $P^* \geq 1$, oscillation was seen at the vicinity of flame holder as the value dropped to $P^* = 0.7$, and the intensity and amplitude of the oscillation around the flame holder were seen as increased with decreasing pressure index. From the schlieren visualization, the formed flames correspond to wrinkled laminar regime.

Fig. 5 shows the averaged emission index of nitric oxide as functions of the pressure index and the equivalence ratio. Emission index decreased with decreasing pressure index for overall equivalence ratio conditions for $P^* < 1$ but kept constant for $P^* \geq 1$. NO_x reduction rates were almost identical for $P^* < 1$, regardless of the equivalence ratio, but the $EINO_x$ values showed different levels with variation of the equivalence ratio for $P^* \geq 1$. $EINO_x$ was reduced monotonously at a rate of almost 0.4 g/10 kPa as the pressure index decreased. This NO_x reduction is ascribed to the enlarged flame length due to the decrease of the combustor pressure, as shown in Fig. 3. For $P^* \geq 1$ conditions, the level of NO_x emission decreased with increasing equivalence ratio. However, for $P^* < 1$ conditions, the emission index was reversed, indicating that the combustion characteristics were quite different for $P^* \geq 1$ and $P^* < 1$. The reason will be discussed later.

Fig. 6 shows the mean temperature distribution with variations of pressure index and equivalence ratio. Mean temperature was measured at one-half length cross-section of the flame length for each experimental condition. For all experimental conditions, the mean temperature was maximum at the center of the combustor and it decreased with radial direction. However, quite different tendency was observed between $P^* \geq 1$ conditions and $P^* < 1$ conditions. A narrow high-temperature region was shown for the $P^* \geq 1$ conditions. On the other hand, the temperature distribution was relatively uniform and wide in the $P^* < 1$ conditions. For a relatively lean combustion condition, the pressure index had a large influence on the temperature distribution. For $P^* \geq 1$ conditions, the mean temperature decreased slightly near center of the combustor, and then it decreased dramatically at the $R = 6$–12 mm region. On the other hand, for $P^* < 1$ conditions, the mean temperature decreased

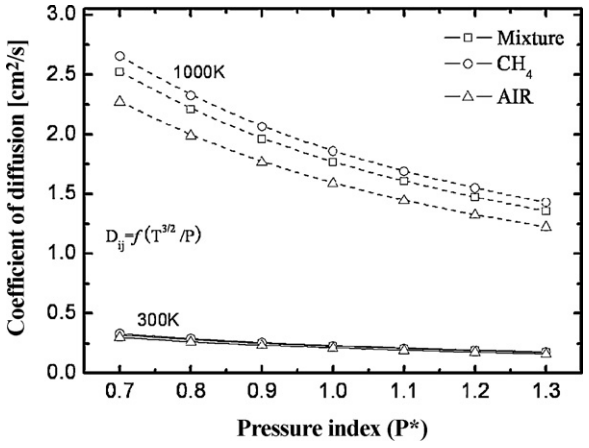

Fig. 9. Coefficient of diffusion as function of pressure index.

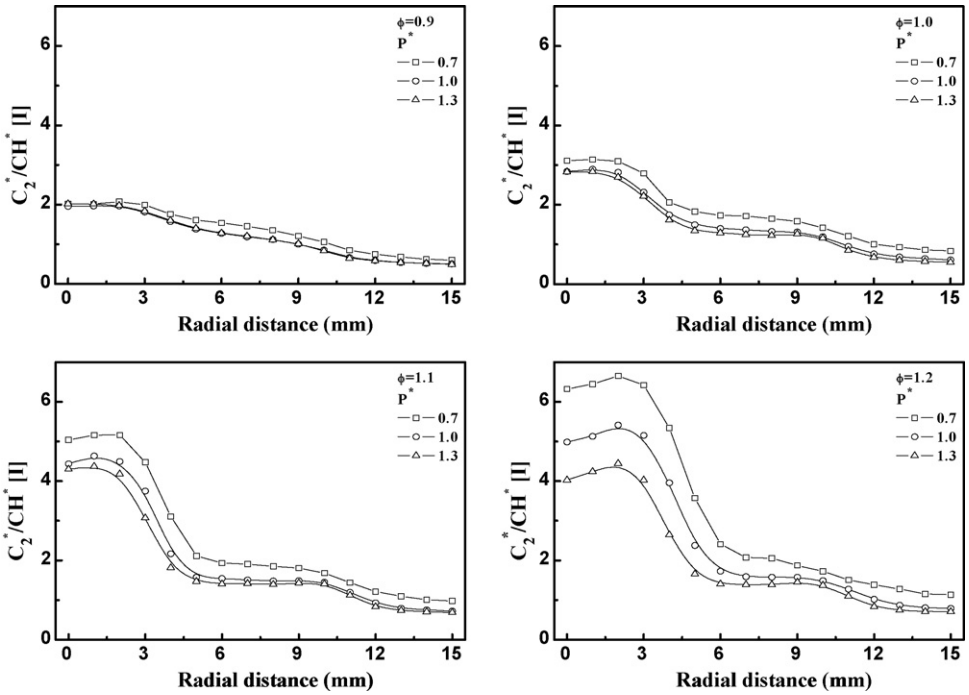

Fig. 10. Correlation of chemiluminescence intensity ratios (C_2^*/CH^*) with pressure index and equivalence ratio.

monotonously, and it showed a relatively low value compared with that for the $P^* \geq 1$ condition. This relatively uniform and low temperature distribution is ascribed to the enlarged flame length, hence low nitric oxide emission. Note that the temperature difference between $P^* \geq 1$ and $P^* < 1$ conditions became smaller with increasing equivalence ratio.

3.2. Relationship between combustor pressure and local heat release rate

Fig. 7 shows the direct photograph of a flame ($\Phi = 1.0$, $P^* = 1.0$) and representative time-series signals of the CH^* chemiluminescence intensity. The mean intensity of CH^* chemiluminescence at the reaction zone was higher than those at the inner flame region and the outer flame region. This result shows that strong reaction emits high intensity chemiluminescence. The local chemiluminescence intensities were measured at 1/2 of the flame length where the pilot flame did not exist.

Fig. 8 shows the mean intensities of OH^*, CH^* and C_2^* chemiluminescences at the flame-front for pressure index (P^*) of 0.7–1.3 and equivalence ratios (Φ) of 0.9–1.2. The OH^*, CH^* and C_2^* emission intensities of the hydrocarbon flames are functions of the local heat release rate. The peak intensity was at the vicinity of the combustor center for each condition, and it decreased with radial direction. This was similar to the results of the mean temperature distribution. The peak value of each radical chemiluminescence increased with increasing pressure index for $\Phi \leq 1$. In the case of $\Phi > 1$, the results obtained were contrary to those of the $\Phi < 1$ condition. For $\Phi > 1$ conditions, the reaction intensity became stronger with decreasing pressure index. Fig. 9 shows the coefficient of diffusion as a function of the pressure index. The gas diffusion velocity is accelerated at the low-pressure condition. The diffusion coefficient (D_{ij}) increased with decreasing pressure, and it would appear that $D_{ij} \alpha T^{3/2}/P$ [4,22–24]. Note that the diffusion coefficient of CH_4 is higher than those of the mixture and air. The difference of diffusion coefficient between Ch_4 and air was 0.21 for $P^* = 1.3$, 0.27 for $P^* = 1.0$ and 0.39 for $P^* = 0.7$. In this result, the strong reaction at the low-pressure index was ascribed to the accelerated diffusion velocity of the unburned fuel for rich conditions. The higher NO_x emission at low-pressure index in Fig. 5 and reduction of the temperature difference between $P^* < 1$ and $P^* > 1$ at the rich condition in Fig. 6 can be explained by this phenomenon.

The relationship between the C_2^*/CH^*, which indicates the relative local equivalence ratio was investigated with the pressure index at the local flame front, as shown in Fig. 10. C_2^*/CH^* ratio showed almost the same value for $\Phi = 0.9$, regardless of the pressure index, and C_2^*/CH^* at $P^* = 0.7$ became larger with increasing equivalence ratio. This results shows that unburned fuel from primary flame can be effectively reacted with surrounding air by decreasing the combustor pressure to below the atmospheric pressure. The reverse of $EINO_x$ at $P^* = 0.7$ as shown in Fig. 5 resulted from the enhanced diffusion velocity of the fuel.

4. Conclusions

In this study, the flame structure and combustion characteristics with the variation of the combustor pressure from −30 kPa to 30 kPa (gage pressure) were investigated by visualization, mean temperature and NO_x emission measurements. The reaction characteristics were analyzed by measurements of CH^*, C_2^* and OH^* chemiluminescence intensities. The findings are summarized as below:

1. The combustion characteristics with the variation of the combustor pressure could be analyzed effectively by measurement of CH^*, C_2^*, OH^* chemiluminescence intensities.
2. The flame structure and combustion characteristics were largely affected by the combustor pressure.
3. Reaction intensity in terms of the pressure index showed an opposite tendency with the variation of the equivalence ratio.
4. Lower pressure than the atmospheric pressure enhanced the combustion reaction with increasing diffusion velocity of unburned fuel for rich conditions.

Acknowledgement

This work supported by research project of the Pusan Clean Coal Center Research Grant.

References

[1] H.H. Liakos, M.A. Founti, N.C. Markatos, Appl. Thermal Eng. 20 (1999) 925–940.
[2] M. Metghalchi, J.C. Keck, Combust. Flame 38 (1980) 143–154.
[3] D.D. Thomsen, Combust. Flame 119 (1999) 307–318.
[4] H. Kobayashi, Exp. Thermal Fluid Sci. 26 (2002) 375–387.
[5] P.G. Alerfens, Y. Hardalupas, A.M.K.P. Taylor, K. Ishii, Y. Urata, Combust. Flames 136 (2004) 72–90.
[6] T.M. Muruganaadam, B. Kim, R. Olsen, M. Patel, B. Romig, J.M. Seitzman, 39th AIAA/ASME/SAE/ASEE Joint Propulsion Conference and Exhibit, 2003, p. 4490.
[7] S.-Y. Lee, S. Seo, J.C. Broda, S. Pal, R.J. Santoro, Combust. Inst. 28 (2000) 775–782.
[8] N.H. Heberle, G.P. Smith, J.B. Jeffries, D.R. Corsley, R.W. Dibble, Appl. Phys. B71 (2000) 733–740.
[9] B. Higgins, M.Q. McQuary, F. Lacas, J.C. Rolon, N. Darabiha, S. Candel, Fuel 80 (2001) 67–74.
[10] B. Higgins, M.Q. McQuary, F. Lacas, S. Candel, Fuel 80 (2001) 1583–1591.
[11] Y. Ikeda, J. Kojima, T. Nakajima, 40th Aerospace Science Meeting and Exhibit, 2002, p. 0193.
[12] Y. Ikeda, J. Kojima, H. Hashimoto, T. Nakajima, 40th Aerospace Science Meeting and Exhibit, 2002, p. 0191.
[13] N. Docquier, S. Belhalfaoui, F. Lacas, N. Darabiha, C. Rolon, Combust. Inst. 28 (2000) 1765–1774.
[14] T. Chou, D.J. Patterson, Combust. Flames 101 (1995) 45–57.
[15] J. Kojima, Y. Ikeda, T. Nakajima, Combust. Inst. 28 (2000) 1757–1764.
[16] Y. Ikeda, J.L. Beduneau, Combust. Inst. 30 (2005) 391–398.
[17] G.-M. Choi, J.-S. Yang, D.-J. Kim, M. Tanahasi, T. Miyauchi, Thermochim. Acta 455 (2007) 34–39.
[18] T.W. Lee, T. Wang, Combust. Flames 121 (2000) 378–385.
[19] K. Hase, Y. Kori, Fuel 75 (1996) 1509–1514.
[20] J. Kojima, Y. Ikeda, T. Nakajima, 36th AIAA/ASME/SAE/ASEE Joint Propulsion Conference and Exhibit, 2000, p. 3394.
[21] Y. Ikeda, J. Kojima, T. Nakajima, F. Akamatsu, M. Katsuki, Combust. Inst. 28 (2000) 343–350.
[22] J.O. Hirschfelder, C.F. Curtiss, R.B. Bird, Mol. Theory Gases Liquids 4 (1967) 514–610.
[23] R.C. Reid, J.M. Prausnitz, B.E. Poling, The Properties of Gases and Liquids, vol. 4, 1986, pp. 577–632.
[24] H. Kobayashi, T. Nakashima, T. Tamura, K. Maruta, T. Niioka, Combust. Flames 108 (1997) 104–117.